Applied Catalysis B: Environmental 94 (2010) 248–253

Contents lists available at ScienceDirect

Applied Catalysis B: Environmental

journal homepage: www.elsevier.com/locate/apcatb

Dependence of photocatalytic activities upon the structures of Au/Pd bimetallic nanoparticles immobilized on TiO_2 surface

Yoshiteru Mizukoshi [a,*], Kazuhisa Sato [b], Toyohiko J. Konno [b], Naoya Masahashi [a]

[a] Osaka Center for Industrial Materials Research, Institute for Materials Research, Tohoku University, 1-2 Gakuen-cho, Naka-ku, Sakai, Osaka 599-8531, Japan
[b] Institute for Materials Research, Tohoku University, 2-1-1 Katahira, Aoba-ku, Sendai, Miyagi 980-8577, Japan

ARTICLE INFO

Article history:
Received 23 September 2009
Received in revised form 20 November 2009
Accepted 21 November 2009
Available online 27 November 2009

Keywords:
Photocatalyst
Promotional effect
Sonochemistry
Nanostructure

ABSTRACT

Bimetallic nanoparticles with a Au-core/Pd-shell structure were prepared and successfully immobilized on a TiO_2 surface using sonochemical method. When immobilizing the core/shell structured bimetallic nanoparticles with a Au/Pd molar ratio of 25/75, TiO_2 showed the highest activity for the photochemical H_2 evolution from ethanol aqueous solution. The activities of other two types of photocatalysts with the same Au/Pd molar ratio, TiO_2 immobilizing the mixture of Au and Pd monometallic nanoparticle, and TiO_2 immobilizing Au/Pd random alloy nanoparticles wherein Au and Pd atoms homogeneously located, were also evaluated. The dependence of the photocatalytic activities on the nanostructures of the immobilized bimetals was confirmed.

1. Introduction

Photocatalysts are, in effect, a transducer which transforms light energy into chemically reactive species. For example, anatase titanium dioxide (TiO_2) operates when illuminated with ultraviolet light at wavelengths shorter than 387 nm. This causes photogenerated holes and electrons to migrate to the surface, where they oxidize or reduce species, respectively. However, the recombination of the charge carriers causes a noticeable reduction in the photoactivity [1]. The immobilization of noble metal nanoparticles has been used to inhibit this recombination wherein the photogenerated electrons are trapped in the immobilized noble metal improving the photocatalytic activity. For example, Pt nanoparticles have been immobilized on the surface of TiO_2 using a sonochemical method [2]. The sonochemically decorated photocatalysts showed higher activity than photocatalysts modified by the conventional impregnation method. This was attributed to the cleaner TiO_2 surface and more homogeneous dispersion established by the use of ultrasound.

In the present study, the promotional effect of Au/Pd bimetallic nanoparticles immobilized on TiO_2 photocatalysts has been investigated. The catalytic activities of Au/Pd alloys in the absence of light illumination have already been extensively studied [3–5]. The synergistic effects of the addition of Au to Pd in enhancing the overall catalytic activity, selectivity, and stability of the catalyst has been of some interest. Chen et al. investigated the effect of Au using acetoxylation of ethylene and concluded that the critical reaction site for vinyl acetate consisted of two noncontiguous Pd monomers suitably spaced by Au [6]. Guczi et al. reported the slight synergetic effect of Au/Pd alloy in the CO oxidation catalyzed by Au/Pd bimetallic nanoparticles immobilized on TiO_2 [7]. The synergistic effects were not observed when silica was used instead of TiO_2. Hutching and coworkers reported the direct synthesis of hydrogen peroxide [8,9] and solvent-free oxidation of primary alcohols [10,11] when catalyzed by Au/Pd bimetallic particles. Although the addition of Au to enhance the catalytic activities has been discussed based on the stability, geometric structures, etc., a detailed mechanism has not been elucidated.

The sonochemical preparation of Au-core/Pd-shell bimetallic nanoparticles has also been reported [12]. These bimetallic nanoparticles have an average diameter less than 10 nm, with a Pd-shell less than 2 nm thick. This corresponds to only a few layers of Pd atoms. A blue shift in the Au plasmon absorption peak was observed in the spectra of the aqueous dispersion containing Au-core/Pd-shell bimetallic nanoparticles, indicating that the electron density in the Au-core had increased and the Pd-shell possessed a relatively positive charge [13]. Consequently, the Au-core/Pd-shell bimetallic nanoparticles have shown superior catalytic activities for the hydrogenation of olefins as compared with a mixture of Au and Pd monometallic nanoparticles. This is probably due to the electrical affinity of the double bonds of the olefins to the positively charged Pd-surface [14].

If photogenerated electrons are trapped in the Au-core/Pd-shell bimetallic nanoparticles which have been immobilized on TiO_2,

* Corresponding author. Tel.: +81 0 72 254 6372; fax: +81 0 72 254 6372.
E-mail address: mizukosi@imr.tohoku.ac.jp (Y. Mizukoshi).

0926-3373/$ – see front matter © 2009 Elsevier B.V. All rights reserved.
doi:10.1016/j.apcatb.2009.11.015

and they are localized in the Au-core, the photocatalytic activity of TiO_2 should be improved due to the inhomogeneous distribution of electrons. However, studies on the preparation of photocatalysts with immobilized core/shell nanoparticles and their photocatalytic activity have been quite limited [15–17]. In the present study, TiO_2 photocatalysts with immobilized Au/Pd bimetallic nanoparticles have been prepared by a sonochemical method. The photocatalytic activities were evaluated by H_2 evolution from ethanol aqueous solution, which is a useful model reaction involving photogenerated electrons. The dependence of the photocatalytic activity upon the nanostructure of the immobilized bimetallic nanoparticles was also investigated.

2. Experimental method

2.1. Materials

Noble metal complexes (Na_2PdCl_4, $HAuCl_4$), polyethylenegrycol monostearate ($n \cong 40$, PEG-MS) and ethanol were purchased from Wako Pure Chemicals and used without further purifications. Aeroxide TiO_2 P-25 powder was obtained from Nippon Aerosil.

2.2. Preparation and immobilization of the bimetallic nanoparticles

The preparation of the core/shell nanoparticles immobilized on TiO_2 was conducted in two steps, the preparation, and the immobilization of the core/shell nanoparticles on TiO_2. 50 mL of an aqueous solution of the appropriate noble metal complexes and PEG-MS (0.4 mM) was prepared. The total concentration of the noble metal complexes was 1.0 mM in all cases. Separate preparations synthesized nanoparticles with Au/Pd molar ratios of 0/100, 25/75, 50/50, 75/25, and 100/0. The solution was purged with Ar gas, which was suitable to obtain greater sonochemical effects [18], and then irradiated with ultrasound using a multiwave ultrasonic generator (KAIJO, TA-4021, 200 kHz, 6 W/cm^2) connected to a PZT oscillator. Sonication was carried out in a temperature controlled water bath at 20 °C. The sonochemical reduction method generates the required reducing agents *in situ* by the effects of the ultrasound [12,14,19,20]. Tiny hot spots can form under high-power ultrasound irradiation, causing some organic compounds such as alcohols, surfactants, or water-soluble polymers to be thermally decomposed into radicals [18]. Some of these radicals can reduce noble metal ions in solution to form nanoparticles. 30 min was required to complete the reduction of the noble metal ions. When the reduction was completed, the solution had become dark brown. Subsequently, TiO_2 powder (0.64 g) was added into the solution and sonication was continued for 30 min. The photocatalyst was collected by filtration, rinsed and dried. The TiO_2 powder had taken up the color of the noble metal nanoparticles and the filtrate was colorless and transparent, suggesting that all of noble metal nanoparticles had been successfully immobilized on the TiO_2. The sonochemical immobilization of the prepared Au/Pd nanoparticles is considered to come from the shock wave generated during the collapse of cavitation bubbles. This is supported by the study of Suslick and Doktycz, reporting that the shock waves induced the inter-particle collisions with a high velocity [21]. Details of the sonochemical immobilization of noble metal nanoparticles on TiO_2 surface has been previously reported elsewhere [2].

2.3. Characterization of the photocatalysts

The morphologies and nanostructures of the TiO_2 were analyzed by scanning-transmission electron microscopy (STEM, FEI Titan 80-300 operated at 300 kV) equipped with a high-angle annular dark field (HAADF) detector. A beam convergence angle of 10 mrad and a detector inner angle higher than 60 mrad were used for HAADF-STEM imaging. The diffusion reflection spectra of the prepared photocatalysts were measured with a UV–vis spectrophotometer (JASCO V-550) equipped with an integration sphere. X-ray photoelectron spectroscopy (XPS) measurements were conducted with an electron spectrometer (ESCA1600, Ulvac-Phi) equipped with monochromated Al-K_α radiation.

2.4. Evaluation of the photocatalytic activities

The photochemical evolution of H_2 from ethanol aqueous solutions was employed as a model reaction to evaluate the photocatalytic activities. The detailed reaction pathway has been reported elsewhere [22]. The photocatalyst powder was dispersed in a 5 M ethanol aqueous solution using a conventional ultrasonic cleaning bath. After purging with Ar, the sample was illuminated with a xenon lamp. For the duration of the irradiation, the generated H_2 was periodically determined using GC/TCD (Shimadzu GC-2014) equipped with a Shincarbon ST (Shinwa Kako, 4 m × 3 mm I.D.). The xenon lamp (Asahi Spectra, MAX-302, 300 W) employed in the present study was equipped with mirror modules, so that light wavelengths from 250 to 385 nm (UV), and 385 to 740 nm (VIS) could be selectively used as shown in Fig. S1 of the supplementary materials. The intensities of the illuminated UV and VIS were 12.7 and 151 mW/cm^2, respectively.

3. Results and discussion

Fig. 1 shows the amounts of evolved H_2 over the TiO_2 with immobilized Au/Pd nanoparticles. The catalyst with 75 mol% of Pd

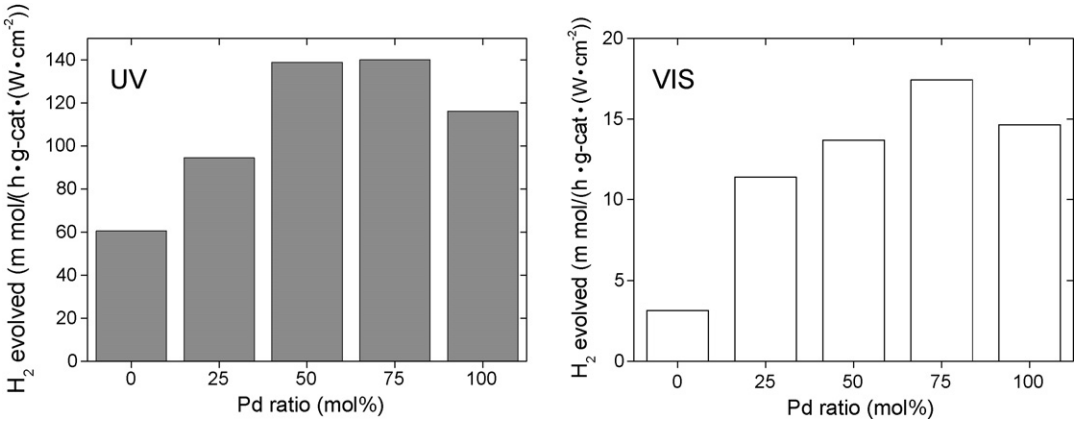

Fig. 1. Amounts of photochemically evolved H_2 over Au/Pd bimetallic nanoparticle immobilized on TiO_2.

showed the highest activities among the investigated samples. According to previous studies on the catalytic activity dependences of the Au/Pd ratio on the reaction in the dark, the sonochemically prepared Au-core/Pd-shell bimetallic nanoparticles exhibit the highest activity at a molar ratio of 20/80 for the hydrogenation of 4-pentenoic acid [14]. According to Sarkany et al., a Au/Pd molar ratio of 20/80 in a core/shell structured nanoparticles exhibited the highest catalytic activity for the hydrogenation of acetylene [5]. Ishihara et al. also reported that bimetallic nanoparticle of Au/Pd ratio of 19/81 immobilized on rutile TiO_2 showed superior performance for hydrogen peroxide synthesis by O_2 oxidation with H_2 [23]. These ratios are similar to the ratio obtained here.

H_2 evolution was detected only when the catalyst was illuminated (Fig. S2 in the supplementary material). H_2 was also not evolved when pure water was used as solvent, and when Al_2O_3 was used as substrate instead of TiO_2 (see Figs. S3 and S4). These results show that H_2 is photochemically generated from ethanol, and not by a dark reaction catalyzed by the immobilized noble metals. When noble metals are in contact with an n-type semiconductor like TiO_2, the excited electrons of TiO_2 migrate to the noble metals. The bimetallic nanoparticles containing large amounts of Pd can accept electrons more effectively, as Pd has a larger work function than Au [24,25]. However, in the present study, the amounts of H_2 did not increase linearly with the increase in Pd. Presumably, this high activity is attributable to the structure of the bimetallic nanoparticles, as well as their composition.

TEM images of the prepared photocatalysts are shown in Fig. 2(a). As indicated by arrows, the fine particles in strong contrast, which are probably due to noble metals, can be recognized together with coarse particles in weak contrast, which are probably TiO_2. Fig. 2(b) is a TEM image of a small particle immobilized on TiO_2, and Fig. 2(c) is the corresponding HAADF–STEM image of the same particle. In HAADF images, the contrast of the observed objects is proportional to the square of the atomic numbers, meaning heavy atoms are bright when compared with light atoms. The atomic numbers of Au, Pd, Ti are 79, 46, and 22, respectively. In Fig. 2(c), the core is brighter than the shell. Therefore, it is concluded that the core is the heavier Au and the shell is Pd. High resolution HAADF–STEM images of immobilized bimetallic nanoparticles (Fig. 2(d)) shows typical multiple twined structure which are composed of several segments to form icosahedrons, decahedrons or a truncated structure [26]. The boundaries of the segments are denoted in the image.

In UV–vis absorption spectra of Au-core/Pd-shell bimetallic nanoparticle, with the increment of the Pd content in core/shell particles, the surface plasmon peak of Au tends to shift toward lower wavelength region (Fig. S5(a)) [12,14]. Mulvaney et al. reported that the blue shift of Au plasmon peak results from the increase of electron density in Au-core due to electron donation from shell material to Au-core [13]. When the core/shell structured bimetallic particles are immobilized on TiO_2 surface, the photogenerated electrons are also anticipated to be localized in the Au-core and to inhibit the recombination of the charge carriers, resulting in high photocatalytic activities. The blue shift indicating the electron accumulation was not observed for the mixtures of monometallic particles of Au or Pd (Fig. S5(b)). Meanwhile, in the case of core/shell particles with higher Pd contents, thicker Pd-shell is supposed to effectively shields photogenerated electrons from the recombination with holes. Therefore, it is thought that core/shell particles containing more Pd show higher promotional effect on TiO_2 photocatalytic activities.

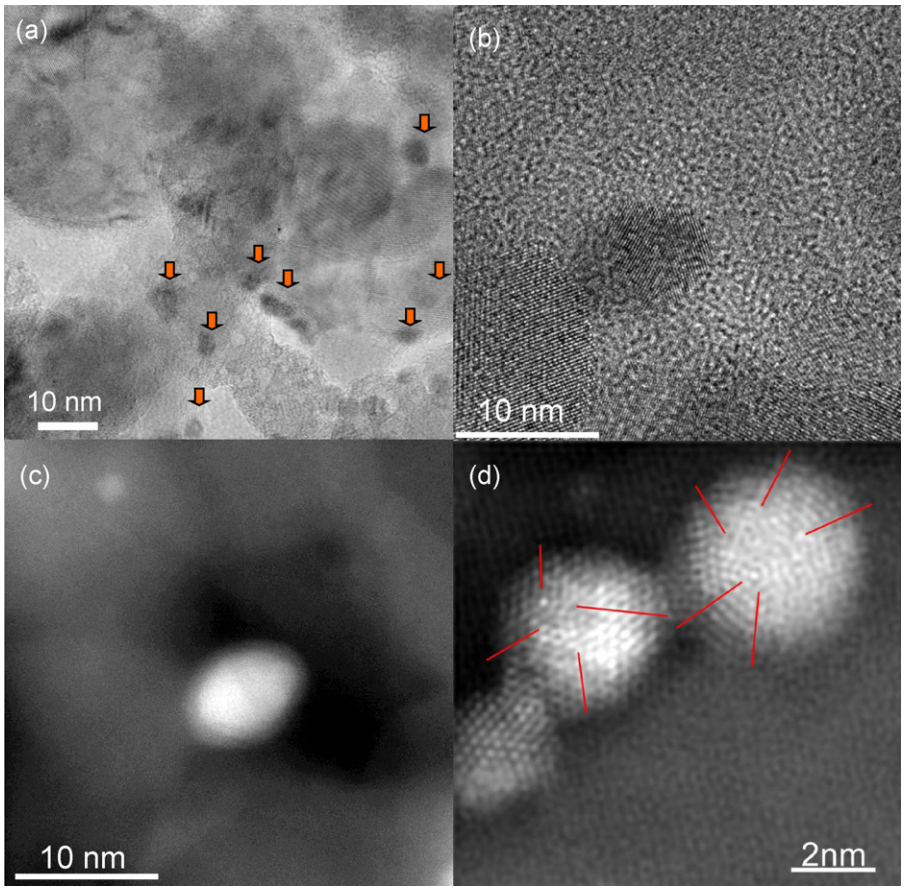

Fig. 2. TEM images of sonochemically prepared Au25/Pd75 (mol%) core/shell nanoparticles immobilized on TiO_2: (a) TEM, (b) HR-TEM, (c) HAADF–STEM, and (d) high resolution HAADF–STEM.

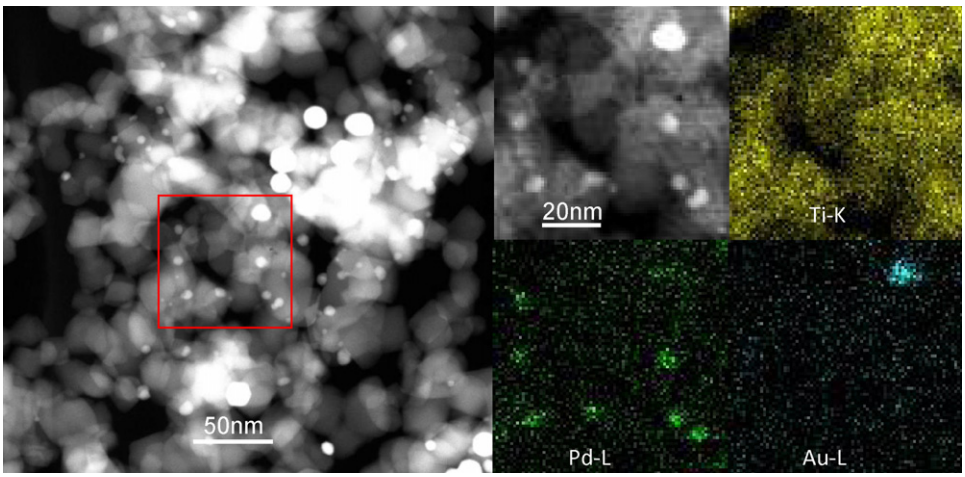

Fig. 3. HAADF–STEM images of separately prepared Au and Pd monometallic nanoparticle immobilized on TiO_2 and the corresponding EDS mappings.

In order to compare the promotional effects of the core/shell bimetallic nanoparticles with other catalysts, two catalysts were independently prepared. First, monometallic Au and Pd nanoparticles were separately prepared by the same sonochemical method and a mixture of these particles was immobilized on TiO_2. HAADF–STEM images of this sample and the EDS maps of the marked area are shown in Fig. 3, indicating that the Au and Pd monometallic nanoparticles have been successfully immobilized on TiO_2.

The core/shell nanoparticles immobilized photocatalysts were annealed at 400 °C for 1 h under a H_2 atmosphere, and the annealed photocatalyst was used as a second reference. Annealing

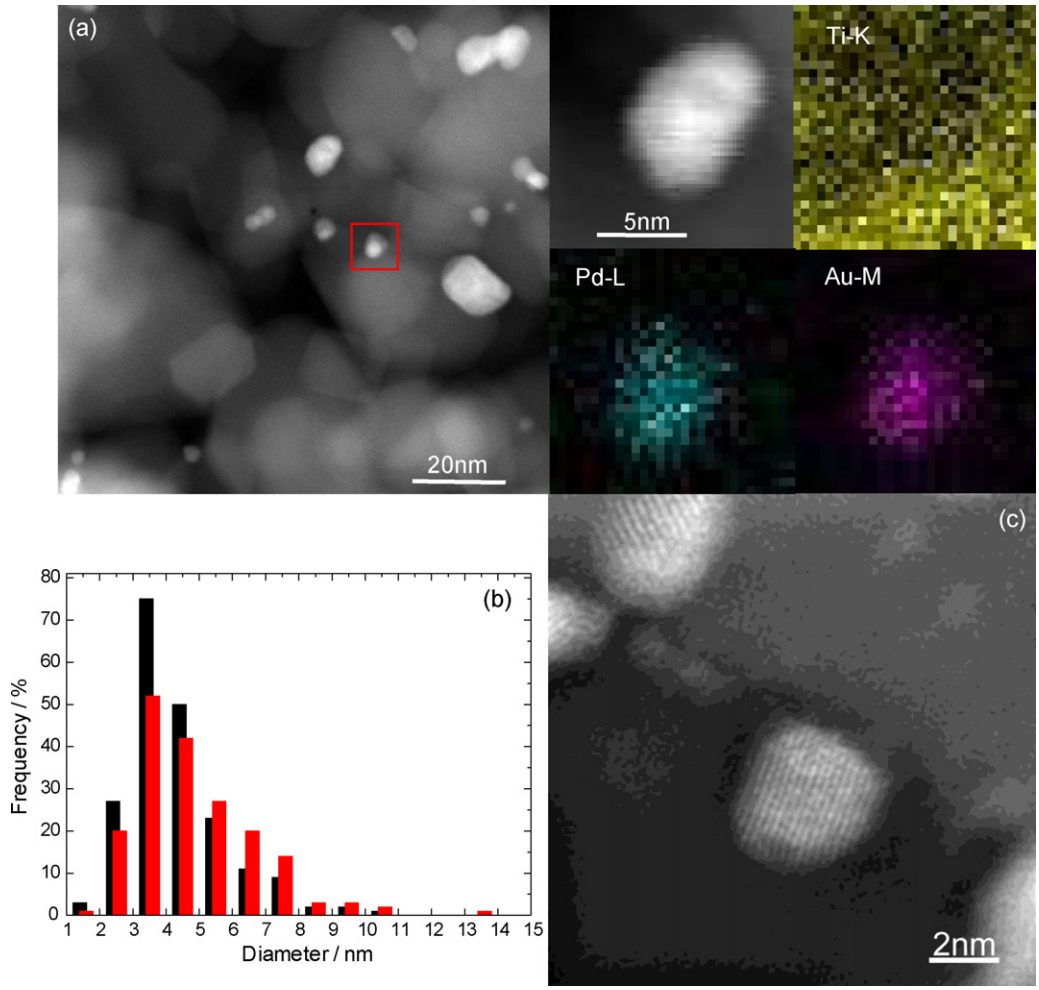

Fig. 4. (a) HAADF–STEM images of annealed core/shell nanoparticles immobilized on TiO_2, and the corresponding EDS mappings, (b) the size distribution of the immobilized bimetallic nanoparticles before (black) and after (red) annealing, and (c) high resolution HAADF–STEM image of the immobilized nanoparticles. (For interpretation of the references to color in the citation of this figure, the reader is referred to the web version of the article.)

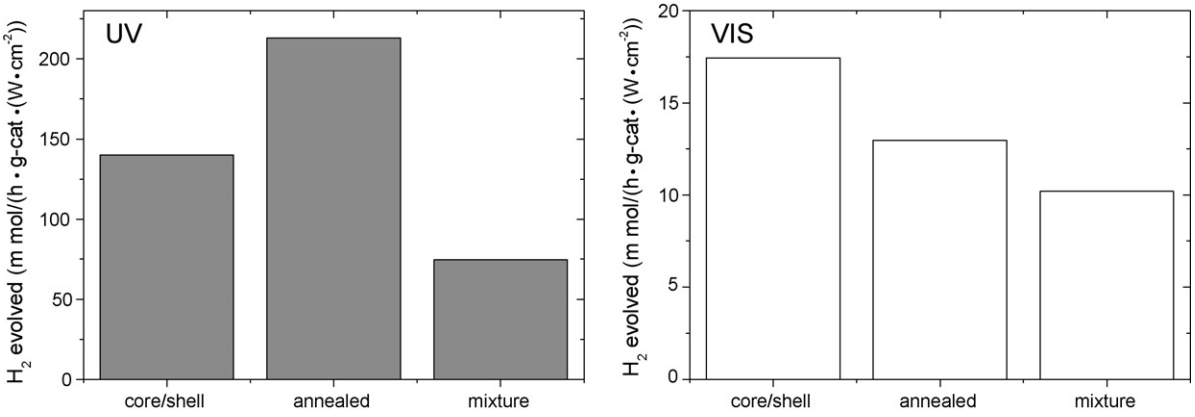

Fig. 5. H_2 evolution under UV and VIS light illumination over the Au/Pd nanoparticles immobilized on TiO_2.

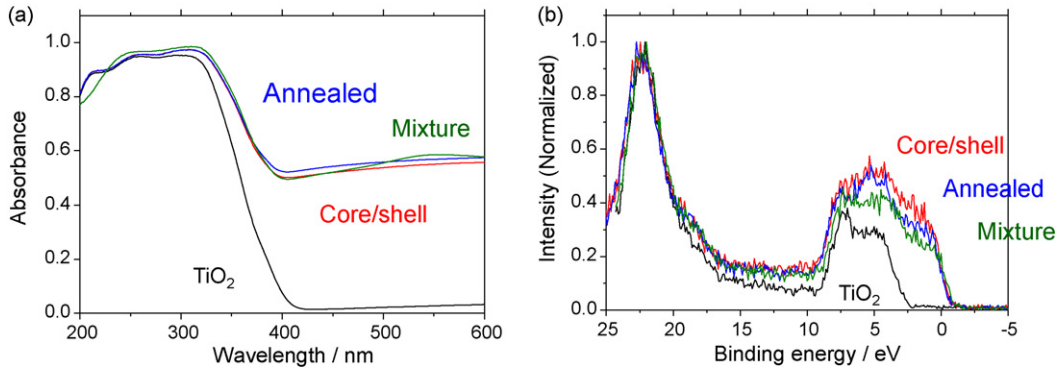

Fig. 6. (a) Diffusion reflection spectra and (b) XPS spectra of the photocatalysts immobilizing Au/Pd bimetallic nanoparticles.

of the sonochemically prepared Au-core/Pd-shell nanoparticles embedded in silica matrix has been reported previously [27]. According to the studies by XRD and EXAFS, the core/shell structure was broken by annealing resulting in a random alloy, wherein the Au and Pd atoms have been homogeneously distributed. An HAADF–STEM image of the annealed catalyst together with EDS maps of the marked area are displayed in Fig. 4. Au and Pd signals occur in almost the same area. Since the size of the noble metal nanoparticles immobilized on TiO_2 affects the promotional effects, it is desirable to maintain their nanosize upon annealing. The histogram of the size distributions of the immobilized bimetallic nanoparticles is also shown in Fig. 4. The average diameters of the particles are 4.2 and 4.8 nm for the samples before and after annealing, respectively. While the annealed sample showed a slightly broader size distribution as compared with the crude sample, there was no direct evidence of growth upon annealing. On the other hand, the high resolution HAADF–STEM images showed the multiple twined structures of the immobilized bimetallic nanoparticles disappeared upon annealing.

The prepared photocatalysts consisting of core/shell nanoparticles, monometallic mixtures, or annealed random alloy particles immobilized on TiO_2 were analyzed by ICP, resulting in no substantial differences in Au, Pd and Ti contents among them. Fig. 5 shows the amount of evolved H_2 by each of the photocatalysts. The H_2 evolution varied with the structures of the bimetallic nanoparticles. The core/shell immobilized photocatalyst exhibits the highest performance under VIS illumination, whereas the annealed sample exhibits the highest performance of the photocatalysts under UV illumination. The performance of the mixture immobilized on $TiO_2$was inferior under all tested illumination conditions.

The diffusion reflection spectra of Au/Pd nanoparticle immobilized on TiO_2 are shown in Fig. 6(a). The spectra of the Au/Pd nanoparticles immobilized on TiO_2 show an increase in the absorbance at wavelengths longer than 400 nm. The observed band gap narrowing (core/shell: 3.23 eV, annealed: 3.22 eV, mixture: 3.20 eV, TiO_2 (P-25): 3.30 eV) is attributed to the immobilized bimetallic nanoparticles. This is supported by the XPS spectra as shown in Fig. 6(b). By immobilizing the bimetallic nanoparticles, the energy level of the valence bands of the photocatalysts is shifted to lower energy. These data support the band gap narrowing originating in the immobilized Au/Pd nanoparticles. This results in more absorption at longer wavelengths and causes an improvement in the photocatalytic activities under VIS illumination. However, a link between these spectral features and the observed photocatalytic performances has not been proved.

The restrictions on back reactions or side reactions could affect the photocatalytic activities for H_2 evolution. Domen et al. reported an excellent promotional effects of noble metal/Cr_2O_3 core/shell nanoparticles for the photocatalytic overall water splitting [15]. The core/shell nanoparticles selectively donate photogenerated electrons to protons, and the Cr_2O_3 shell restricts the reaction between the photocatalytic products, H_2 and O_2. This improves the efficiency of the evolution of H_2 and O_2 from water molecules. In the present Au-core/Pd-shell particles, selective H_2 permeability by the Pd-shell might contribute to the selective donation of photogenerated electrons to protons, and the resultant highly promoted photocatalysis of H_2 from aqueous ethanol solutions [28,29].

4. Conclusions

The photocatalytic activities of TiO_2 immobilizing Au/Pd bimetallic nanoparticles prepared by sonochemical reduction method were explored. The promotional effects of the immobilized nanoparticles depended on the nanostructure, suggesting that the functions of the photocatalysts could be controlled through control of the nanostructure of the immobilized bimetallic particles. Further studies to elucidate the mechanism are in progress.

Acknowledgements

The authors wish to thank Emeritus Prof. Y. Maeda (Osaka Prefecture University) for his valuable comments and his critical reading of the manuscript. We wish to acknowledge Ms. Y. Matsuda (IMR, Tohoku University) and Mr. N. Shima (Nagasaki University) for their helpful assistances in the evaluation of the photocatalytic activities, Dr. N. Ohtsu (Kitami Institute of Technology) for XPS experiments, and Dr. S. Tanabe (Nagasaki University) for his valuable comments. One of the authors (Y.M.) acknowledges the Grant-in-Aid for Young Scientists (B) (No. 20760525) from Japan Society for the Promotion of Science (JSPS).

Appendix A. Supplementary data

Supplementary data associated with this article can be found, in the online version, at doi:10.1016/j.apcatb.2009.11.015.

References

[1] A.L. Linsebigler, G. Lu, J.T. Yates Jr., Chem. Rev. 95 (1995) 735–758.
[2] Y. Mizukoshi, Y. Makise, T. Shuto, J. Hu, A. Tominaga, S. Shironita, S. Tanabe, Ultrason. Sonochem. 14 (2007) 387–392.
[3] E.G. Allison, G.C. Bond, Catal. Rev. 7 (1972) 233–289.
[4] A. Villa, C. Campione, L. Prati, Catal. Lett. 115 (2007) 133–136.
[5] A. Sarkany, P. Hargittai, A. Horvath, Top. Catal. 46 (2007) 121–128.
[6] M. Chen, D. Kumar, C.-W. Yi, D.W. Goodman, Science 310 (2005) 291–293.
[7] L. Guczi, A. Beck, A. Horváth, Zs. Koppány, G. Stefler, K. Frey, I. Sajó, O. Geszti, D. Bazin, J. Lynch, J. Mol. Catal. A 204–205 (2003) 545–552.
[8] J.K. Edwards, B.E. Solsona, P. Landon, A.F. Carley, A. Herzing, C.J. Kiely, G.J. Hutchings, J. Catal. 236 (2005) 69–79.
[9] P. Landon, P.J. Collier, A.F. Carley, D. Chadwick, A.J. Papworth, A. Burrows, C.J. Kiely, G.J. Hutchings, Phys. Chem. Chem. Phys. 5 (2003) 1917–1923.
[10] G. Li, D.I. Enache, J. Edwards, A.F. Carley, D.W. Knight, G.J. Hutchings, Catal. Lett. 110 (2006) 7–13.
[11] D.I. Enache, J.K. Edwards, P. Landon, B. Solsona-Espriu, A.F. Carley, A.A. Herzing, M. Watanabe, C.J. Kiely, D.W. Knight, G.J. Hutchings, Science 311 (2006) 362–365.
[12] Y. Mizukoshi, K. Okitsu, Y. Maeda, T.A. Yamamoto, R. Oshima, Y. Nagata, J. Phys. Chem. B 101 (1997) 7033–7037.
[13] P. Mulvaney, M. Giersig, A. Henglein, J. Phys. Chem. 96 (1992) 10419–10424.
[14] Y. Mizukoshi, T. Fujimoto, Y. Nagata, R. Oshima, Y. Maeda, J. Phys. Chem. B 104 (2000) 6028–6032.
[15] K. Maeda, K. Teramura, D. Lu, N. Saito, Y. Inoue, K. Domen, Angew. Chem. Int. Ed. 45 (2006) 7806–7809.
[16] H. Tada, T. Mitsui, T. Kiyonaga, T. Akita, K. Tanaka, Nat. Mater. 5 (2006) 782–786.
[17] H. Tada, A. Takao, T. Akita, K. Tanaka, Chem. Phys. Chem. 7 (2006) 1687–1691.
[18] T.J. Mason, Sonochemistry, Oxford University Press, New York, 1999.
[19] Y. Mizukoshi, R. Oshima, Y. Maeda, Y. Nagata, Langmuir 15 (1999) 2733–2737.
[20] Y. Mizukoshi, E. Takagi, H. Okuno, R. Oshima, Y. Maeda, Y. Nagata, Ultrason. Sonochem. 8 (2001) 1–6.
[21] S.J. Doktycz, K. Suslick, Science 247 (1990) 1067–1069.
[22] G.R. Bamwenda, S. Tsubota, T. Nakamura, M. Haruta, J. Photochem. Photobiol. A-Chem. 89 (1995) 177–189.
[23] T. Ishihara, Y. Hata, Y. Nomura, K. Kaneko, H. Matsumoto, Chem. Lett. 36 (2007) 878–879.
[24] X. Wang, J.C. Yu, H.-Y. Yip, L. Wu, P.-K. Wong, S.-Y. Lai, Chem. Eur. J. 11 (2005) 2997–3004.
[25] H.B. Michaelson, J. Appl. Phys. 48 (1977) 4729–4733.
[26] Z.-R. Dai, S. Sun, Z.L. Wang, Surf. Sci. 505 (2002) 325–335.
[27] T. Nakagawa, H. Nitani, S. Tanabe, K. Okitsu, S. Seino, Y. Mizukoshi, T.A. Yamamoto, Ultrason. Sonochem. 12 (2005) 249–254.
[28] E. Kikuchi, S. Uemiya, N. Sato, H. Inoue, H. Ando, T. Matsuda, Chem. Lett. 18 (1989) 289–292.
[29] A. Tominaga, Y. Mizukoshi, O. Nakagoe, S. Tanabe, Top. Catal. 52 (2009) 860–864.